ISSN impresa 0717-3644
ISSN online 0718-221X

Maderas. Ciencia y tecnología 2021 (23): 36, 1-16

DOI: 10.4067/s0718-221x2021000100436

CRYSTALLINITY AND IMPACT STRENGTH IMPROVEMENT OF WOOD-POLYLACTIC ACID BIOCOMPOSITES PRODUCED BY ROTATIONAL AND COMPRESSION MOLDING

***Aida Alejandra Pérez-Fonseca*[1]**

https://orcid.org/0000-0003-2443-3882

***Verónica Olimpia Ramírez-Herrera*[2]**

https://orcid.org/0000-0003-0523-1126

***Francisco Javier Fuentes-Talavera*[2]**

https://orcid.org/0000-0002-4386-1092

***Denis Rodrigue*[3]**

https://orcid.org/0000-0002-3969-2847

***José Antonio Silva-Guzmán*[2]**

https://orcid.org/0000-0002-8636-7887

***Jorge Ramón Robledo-Ortíz*[2,♠]**

https://orcid.org/0000-0002-1309-6203

ABSTRACT

Polylactic acid is one of the most used biopolymers due to its overall properties and biodegradability. Nevertheless, polylactic acid has important drawbacks such as brittleness, low thermal stability, and higher cost than most commodity polymers. In order to overcome those disadvantages without compromising biodegradability, the addition of wood particles and thermal annealing on the crystallinity and impact strength of wood-polylactic acid biocomposites were studied. The samples were prepared by compression and rotational molding using two different wood particles: white ash and tzalam. The results showed that thermal annealing at 100 °C, 40 minutes, increased the crystallinity up to 60 % and also improved the thermal stability of polylactic acid and its biocomposites as determined via dynamic mechanical analysis. The specimens not exposed to thermal annealing exhibited important storage modulus loss above 60 °C, which mostly disappeared with the thermal treatment. Furthermore, the impact strength was substantially increased by the thermal treatment. Additionally, accelerated weathering tests showed that the thermally annealed samples had better dimensional stability growing their potential applications over a wider range of conditions.

Keywords: Biocomposites, biopolymers, compression molding, polylactic acid, rotational molding, thermal annealing.

[1]Universidad de Guadalajara, Departamento de Ingeniería Química, Jalisco, México.
[2]Universidad de Guadalajara, Departamento de Madera, Celulosa y Papel, Jalisco, México.
[3]Université Laval, Department of Chemical Engineering and CERMA, Quebec, Canada.
♠Corresponding author: jorge.robledo@academicos.udg.mx
Received: 08.05.2020 Accepted: 20.02.2021

INTRODUCTION

The use of biodegradable polymers has significantly increased over the last years, especially the polylactic acid (PLA) due to its good properties such as high mechanical strength, easy processability, and a wide range of available commercial grades (González-López *et al.* 2018, Altuntas and Aydemir 2019). PLA is a semi-crystalline aliphatic polyester with applications in the agricultural, biomedical, and packaging industries (Kim *et al.* 2007). Its properties are similar to other general-purpose polymers such as polypropylene (PP) and polystyrene (PS), being an excellent material for several fields like electronics, automotive, food, and construction industries (Faludi *et al.* 2013). Nevertheless, PLA has some critical drawbacks such as brittleness, low thermal stability, and higher cost than commodity polymers (Frone *et al.* 2013). Therefore, strategies have been developed to overcome these disadvantages. One example is the addition of natural fibers to produce 100 % biodegradable biocomposites, reducing cost, enhancing thermal stability, and improving some mechanical properties (Pérez-Fonseca *et al.* 2016). On the other hand, natural fibers are biodegradable, non-toxic, and low cost (Adefisan and McDonald 2019). They are also obtained from renewable sources and produce less abrasion than inorganic fillers (Dong *et al.* 2014).

The low crystallinity and brittleness of PLA limit some of its applications (Piekarska *et al.* 2017). In order to increase the crystallinity of polymers, one option is to include nucleating agents like talc, clays, or other similar particles (Yang *et al.* 2015). However, these particles usually decrease the impact strength of biocomposites (Petchwattana *et al.* 2014). Another strategy is to perform a thermal annealing treatment (Ferrer-Balas *et al.* 2001), which consists of placing the samples under controlled temperature and time conditions. For example, Srithep *et al.* (2013) performed thermal annealing on injection molded PLA using different temperatures (65 ºC to 80 ºC) and time intervals (10 min up to 31 h). It was observed that the highest amount of crystallinity (49 %) was obtained at 80 ºC for 30 min. Also, increasing the crystallinity from 16 % to 49 % improved the tensile strength by 17 % and the tensile modulus by 7 %. Mathew *et al.* (2006) prepared PLA-cellulose composites by injection molding and annealed the sample at 80 ºC for three days. It was observed that as crystallinity increases from 19 % to 57 %, there was a substantial improvement in the thermal stability as determined via dynamic mechanical analysis (DMA). Perego *et al.* (1996) also prepared PLA samples by injection molding and applied thermal annealing at 105 ºC for 90 min. They observed an increase in the melting enthalpy (ΔH_m), impact strength, and heat resistance, as well as the tensile and flexural modulus, while the tensile and flexural strengths decreased. Also, Pérez-Fonseca *et al.* (2016) produced biocomposites based on PLA with 10 % to 30 % wt. of pine, coir, or agave fibers. They noted that the storage modulus and impact strength improved when the fiber content was increased, and higher values were reported when the samples were thermally annealed at 105 ºC for 60 min.

So far, most of the studies use injection molding to produce biocomposite samples, and there is very limited literature about PLA-based materials processed by rotational molding. For example, Greco *et al.* (2014), Greco and Maffezzoli (2015) and Greco and Maffezzoli (2017) used PLA (neat and plasticized) for rotational molding and provided information about its processing window (powder coalescence, sintering, and thermal degradation). Then, Cisneros-López *et al.* (2018) successfully produced PLA-agave fiber biocomposites via dry-blending and rotational molding. Due to the absence of shear stresses during processing, the rotomolded samples presented high porosity, compromising the mechanical properties at high fiber content, especially impact strength. More recently, González-López *et al.* (2019) chemically treated agave fibers to modify the PLA-fiber compatibility in rotomolded biocomposites. Although the flexural and tensile properties were improved, the impact strength did not change with the treatment.

Based on the information available, thermal annealing is an interesting strategy to improve the thermal stability and impact strength of PLA biocomposites because it does not require any additives. In this work, thermal annealing was applied to increase the crystallinity of PLA and its biocomposites based on two different wood fibers (white ash and tzalam). The samples were processed by rotational and compression molding to determine the effect of the processing method. Finally, the effect of thermal annealing was studied for both processing methods. All the samples are characterized in terms of morphological, mechanical, and thermal properties. For more characterization, water absorption and accelerated weathering tests were carried out to get a better idea about these materials' long-term behavior, i.e., during their potential lifetime.

MATERIALS AND METHODS

Materials

The materials used were polylactic acid 3251D supplied by Nature Works LLC (USA) with a MFI of 80 g/10 min (190 ºC/2,16 kg) and a density of 1,24 g/cm^3. Two different types of wood particles were obtained from residues of tzalam wood (*Lysiloma latisiliquum* (L.) Benth) from Chetumal (Quintana Roo, Mexico) and white ash wood (*Fraxinus americana* L.) from the USA provided by Grupo Tenerife S.A. de C.V. (Mexico). Both types of wood residues were ground and sieved to keep only particle sizes of 212 μm to 500 μm.

Biocomposites preparation

The biocomposites were prepared using 15 % and 30 % wt. of wood content. Before their processing, PLA, tzalam (TZ), and white ash (WA) were dried in an oven for 48 h at 65 ºC. The compounds were prepared by dry-blending using a high shear mixer with dull blades (JR Torrey, USA) for 5 min at 3750 rpm (393 rad/s). Then, the blends were processed by compression or rotational molding. Compression-molded (CM) samples were prepared in a laboratory press at 180 ºC using a mold of 12,5 cm × 12,5 cm × 1,8 mm. The material was preheated for 4 min, and the pressure was applied gradually until 200 bar was attained for 6 min. Later, the mold was removed from the press and cooled by forced air for 10 min. On the other hand, rotational-molded (RM) samples were prepared in a laboratory-scale rotational molding machine with a stainless-steel mold of 15 cm × 15 cm × 16 cm and 2,0 mm to 2,5 mm in wall thickness. The following steps were applied: (1) preheating the oven at 300 ºC, (2) loading 350 g of the dry-blended mixture into the mold and heating inside the oven for 24 min with a rotational speed ratio of 4:1 (Cisneros-López *et al.* 2018), (3) cooling with air convection for 24 min, and (4) demolding. Finally, the biocomposites obtained by rotational and compression molding were cut for all the characterization.

Morphology and density

The average particle sizes (L, length; D, diameter) were obtained from optical micrographs using a Nikon DSLR D5100 camera with an AF-S Micro Nikkor 85 mm lens. At least 100 particles were measured using Image-Pro Plus Software. Samples of the biocomposites were cryogenically fractured using liquid nitrogen, and the exposed cross-sections were coated with Au. Micrographs were then taken at different magnifications using a scanning electron microscope (SEM) TESCAN MIRA 3 LMU to characterize the state of wood particles adhesion/dispersion in the matrix. The wood particles and biocomposites' density were determined with a ULTRAPYC 1200e gas pycnometer (Quantachrome Instruments, USA) using nitrogen.

Thermal annealing and DSC analysis

The thermal annealing treatment was carried out in an oven with temperature control by placing the samples on a flat wooden surface. After preliminary trials, it was decided to perform the thermal annealing at 100 ºC for 40 min, which was the conditions that produced the highest crystallinity values. (Note: the code "T" corresponds to thermally treated samples, while the code "U" refers to untreated samples).

The crystallinity (X_c) was measured by differential scanning calorimetry (DSC) analysis in a TA Instruments (USA) Q100. The samples (4-6 mg) were cut from molded specimens to perform a scan between 25 ºC and 200 °C at a heating rate of 10 °C/min under a nitrogen flow of 50 mL/min. The crystallinity was calculated as (Equation 1):

$$X_c(\%) = \frac{\Delta H_m - \Delta H_c}{\Delta H_{ref}} x \frac{1}{x} x\ 100 \quad (1)$$

Where ΔH_m and ΔH_c are the heat of fusion and cold crystallization, respectively, ΔH_{ref} is the theoretical heat of fusion for 100 % crystalline PLA (93 J/g, Mathew *et al.* 2006), and x is the weight fraction of PLA in the biocomposites.

Dynamic mechanical analysis (DMA)

DMA was performed on a TA Instruments (USA) RSA3 using a three-point bending fixture. The temperature was ramped from 40 ºC to 110 ºC at a heating rate of 1,5 °C/min using a frequency of 1 Hz under the auto-tension mode (0,02 % deformation). The test specimen dimensions were 30,0 mm x 12,7 mm x 1,8 mm to 2,5 mm, and the span was 25 mm. For each sample, a minimum of two specimens was analyzed.

Charpy impact strength

The Charpy impact strength tests were performed at room temperature (23 ºC) according to ASTM D6110 (2018) using an Instron Ceast (USA) model 9050 impact tester. The specimens with dimensions of 126 mm x 12,7 mm x 1,8 mm to 2,5 mm were notched 24 h before testing using an Instron Ceast 6897 notcher. The reported values are the average of at least ten specimens.

Tensile and flexural properties

Tensile and flexural properties were measured at room temperature (23 ºC) using a universal testing machine Instron Ceast (USA) model 4411. At least seven specimens were evaluated to obtain average values. According to ASTM D638 (2014), tensile tests were carried out using the type IV specimen and a 5 mm/min crosshead speed. For flexural tests, the ASTM D790 (2017) was followed using specimens of 80 mm x 12,7 mm x 1,8 mm to 2,5 mm with a span of 16 times the samples' thickness and a crosshead speed of 2 mm/min.

Water absorption and accelerated weathering

Water absorption tests were carried out according to ASTM D570 (2018). Five samples of each material with dimensions of 20 mm x 19 mm x 1,8 mm to 2,5 mm were dried and weighed. The samples were submerged in distilled water at 23 ºC. Then, the samples were removed, wiped off with a dry cloth, and weighed. This procedure was repeated until a constant weight was reached. The maximum water absorption (M_∞) was calculated as (Equation 2):

$$M_\infty(\%) = \frac{W_\infty - W_0}{W_0} x100 \quad (2)$$

Where w_∞ is the weight of the sample at the equilibrium and w_0 the initial weight.

The effect of fiber content and thermal annealing on the behavior of the PLA and the biocomposites under weathering conditions was also studied. For this purpose, impact test specimens were subjected to accelerated weathering in a Q-Lab QUV (USA) basic equipment with UVB-313EL fluorescent bulbs. The test was carried out under controlled conditions of exposure to UV radiation, temperature, and humidity, according to ASTM D4329 (2013): UV irradiation (2 h) - condensation (2 h) cycles were applied for 600 h at 60 ºC. The physical appearance, DSC, DMA, and mechanical properties of the weathered (W) specimens were analyzed.

RESULTS AND DISCUSSION

Morphology and density

The average dimensions of the tzalam particles were L = 1263 µm ± 251 µm, D = 471 µm ± 93 µm, with an aspect ratio of 2,7 ± 0,6. Similar values were obtained for white ash particles, with L = 1448 µm ± 366 µm, D = 466 µm ± 86 µm, and an aspect ratio of 3,1 ± 0,8. Figure 1 presents typical SEM images of RM and CM biocomposites for the different wood types and content. As reported previously (Pérez-Fonseca *et al.* 2016), the thermal annealing treatment did not modify the morphology, but the processing method substantially affected the biocomposites structure. In general, voids, gaps, and fiber pull-out are observed due to the poor wood/matrix adhesion. As expected, these defects are more significant in RM samples due to lack of pressure during processing, especially at higher wood content (30 %), where several gaps and higher porosity were observed. The better morphology of CM samples was related to the high pressure applied during processing. This pressure allows higher material compaction producing fewer voids and better wood particles wettability, which, as discussed in the following paragraphs, gave higher density values (Altuntas and Aydemir 2019, Cisneros-López *et al.* 2018).

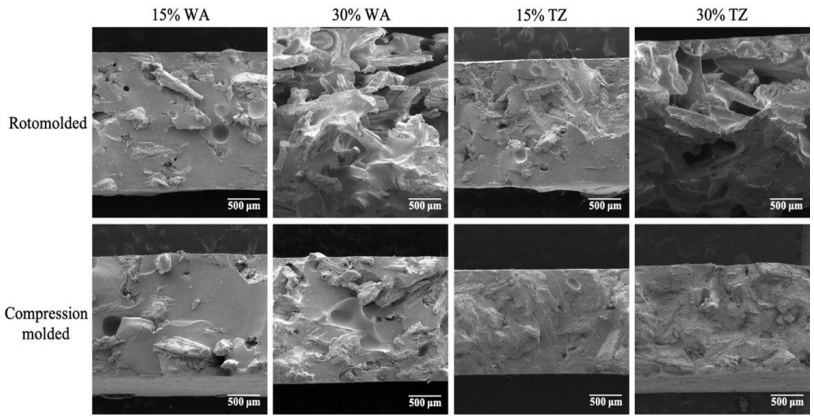

Figure 1: Morphology of RM (first row) and CM (second row) white ash (WA) and tzalam (TZ) PLA biocomposites at different wood content.

The density of the wood particles and the biocomposites are presented in Table 1. The addition of both wood fibers produced small decreases in RM and CM biocomposites' density, even though tzalam and white ash particles densities (1439 kg/m^3 and 1523 kg/m^3, respectively) are higher than the density of neat PLA (1250 kg/m^3). This density reduction is due to voids formation owing to fiber agglomeration, weak fiber-matrix interface, and extractable vaporization (Mahfoudh *et al.* 2013). Also, the decrease in the density is more evident in RM biocomposites due to the rotational molding process's low-shear nature, which produces their morphology observed in Figure 1 (Robledo-Ortíz *et al.* 2020). The treated samples' density is not presented since no changes were observed by the thermal annealing treatment.

Table 1: Density of PLA and its biocomposites produced by compression and rotational molding.

Material	Density (kg/m^3)
Tzalam	1439 ± 4
White ash	1523 ± 4
CM PLA	1250 ± 2
CM 15 % WA	1225 ± 3
CM 30% WA	1234 ± 3
CM 15 % TZ	1244 ± 2
CM 30 % TZ	1251 ± 3
RM PLA	1250 ± 2
RM 15 % WA	1193 ± 3
RM 30% WA	1227 ± 1
RM 15 % TZ	1218 ± 5
RM 30 % TZ	1232 ± 4

WA: white ash; TZ: tzalam

Thermal properties

Semi-crystalline polymers typically have three transitions in a DSC thermogram: the first one corresponds to the glass transition temperature (T_g), the second one to the cold crystallization temperature (T_c), and the third one is the melting temperature (T_m). By applying thermal annealing, the peak corresponding to T_c disappeared, indicating that no crystal formation occurred during heating, and this is a good indicator of a successful thermal annealing process. This behavior can be observed in typical DSC thermograms presented in Figure 2, where thermally treated PLA and biocomposites did not show the T_c peak. Similar results were reported by Mathew *et al.* (2006) and Pérez-Fonseca *et al.* (2016) for PLA-based biocomposites.

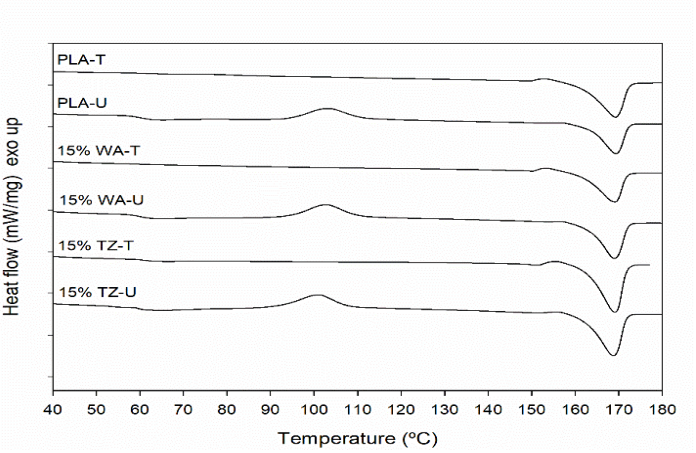

Figure 2: Typical DSC thermograms of PLA and its biocomposites before (U) and after (T) thermal annealing at 100 ºC for 40 min (WA: white ash; TZ: tzalam).

Table 2 reports on the X_c, T_g, T_c, and T_m values of PLA and its biocomposites before and after thermal annealing (100 ºC and 40 min). The initial crystallinity of 19 % and 14 % were obtained for compression molded (CM) and rotomolded (RM) neat PLA. As expected, the wood particles served as nucleation sites for crystals formation (Adefisan and McDonald 2019), increasing X_c for all the biocomposites with a maximum value of 28 % at 30 % wt. of white ash. It is also observed that the crystallinity was higher for compression-molded samples (up to 28 %) than for rotomolded ones (up to 20 %). The latter can be associated with the high pressure used during compression molding, which is absent in rotomolding. This high pressure generated samples with higher density, fewer voids, and better wood particles wettability, as observed in Figure 1 and Table 1, leading to a more efficient and homogeneous crystallization process.

After thermal annealing, the crystallinity of all the materials was substantially increased. The values obtained for neat PLA were 56 % and 54 % for CM and RM, respectively. All the biocomposites achieved crystallinity above 50 %: 60 % for CM and 54 % for RM. For comparison, Pérez-Fonseca *et al.* (2016) obtained crystallinity around 50 % for injection molded PLA and its pine, coir, and agave-based biocomposites, after applying a heat treatment of 105 ºC for 1 h.

Table 2: Crystallinity of PLA and its biocomposites produced by compression and rotational molding before and after thermal annealing.

Process	Thermal annealing at 100 °C	Time (min)	T_g (°C)	T_c (°C)	ΔH_c (J/g)	T_m (°C)	ΔH_m (J/g)	X_c (%)
Compression molding	PLA	0	61	104	29	169	45	19
		40	63	-	0	169	52	56
	15 % WA	0	60	103	25	169	41	20
		40	-	-	0	169	47	60
	30 % WA	0	59	103	17	168	36	28
		40	-	-	0	169	36	56
	15 % TZ	0	59	101	21	169	43	27
		40	62	-	0	169	42	53
	30 % TZ	0	61	97	19	169	34	23
		40	62	-	0	168	39	60
Rotational molding	PLA	0	63	103	28	169	41	14
		40	64	-	0	168	50	54
	15 % WA	0	-	103	20	170	33	16
		40	-	-	0	168	37	47
	30 % WA	0	-	102	16	169	29	20
		40	-	-	0	167	34	52
	15 % TZ	0	-	103	21	168	35	18
		40	-	-	0	169	39	49
	30 % TZ	0	-	102	16	169	29	20
		40	-	-	0	169	35	54

WA: white ash; TZ: tzalam

Before thermal annealing, the glass transition temperatures of the neat matrix produced via RM and CM were 63 ºC and 61 ºC, respectively. Thermal annealing or wood particles' presence did not significantly modify these values: 61 ºC ± 2 ºC. For the cold crystallization temperature, no significant changes were observed due to fiber addition nor thermal annealing, except for the untreated 30 % wt. CM tzalam biocomposites with an important reduction from 104 ºC to 97 ºC. This behavior may indicate a higher nucleation effect accelerating the crystallization process at high TZ content. It has been reported that crystallization can be initiated at the wood-polymer interface (trans-crystallization), but at different surface locations (multiple nucleation sites) depending on the wood particle size and its chemical composition (Mathew *et al.* 2006, Arias *et al.* 2013). All the values obtained for the melting temperatures were around 169 ºC, suggesting that T_m was not affected by the thermal annealing.

Dynamic mechanical analysis (DMA)

Figure 3 presents the storage modulus of the neat PLA and its biocomposites before and after thermal annealing. As earlier discussed, a significant drawback of PLA is its substantial rigidity loss around its glass transition temperature ($\sim$ 60 ºC), limiting its potential applications at a higher temperature. This loss of rigidity can be observed for the PLA processed by both CM (Figure 3b) and RM (Figure 3a), to a point where it was no longer possible to recover the storage modulus at higher temperatures. This softening effect is associated with the α-relaxation of the PLA amorphous regions (Mathew *et al.* 2006, Pérez-Fonseca *et al.* 2016).

When wood particles were added, the materials became more rigid, and less storage modulus loss was observed above the glass transition temperature due to the increased stiffness imparted by the lignocellulosic materials (Way *et al.* 2013). However, the decrease was still important; for example, PLA had a storage modulus of 7 MPa for RM and 5 MPa for CM at 70 ºC, while the maximum values were observed with 30 % wt. of white ash and tzalam with a storage modulus of 47 MPa and 68 MPa for RM, and 88 MPa and 47 MPa for CM, respectively.

Below the glass transition temperature, for example, at 40 ºC, the storage modulus decreased with wood particles' content. At this temperature, the storage modulus of RM neat PLA was 1465 MPa, which was reduced to 890 MPa and 398 MPa with the addition of 15 % and 30 % wt. of white ash, respectively. Similarly, the modulus decreased to 1266 MPa and 580 MPa at 15 % and 30 % of tzalam in RM biocomposites. These results can be related to the wood-PLA incompatibility, lower density, and the limited wettability of the wood particles with the PLA due to the absence of pressure in the rotational molding process (Table 1). On the other hand, for CM samples at 40 ºC, the neat PLA had a storage modulus of 1445 MPa, similar to the RM PLA. Nevertheless, the storage moduli of CM biocomposites were very different from those observed in rotational molding. For instance, the white ash biocomposites storage modulus remained around 1400 MPa, but for 15 % wt. tzalam biocomposite, the storage modulus increased to 1600 MPa (11 % higher than neat PLA). Only at 30 % wt. tzalam, the value decreased to 1100 MPa, probably because at this high wood content once again the state of dispersion and low wood-matrix adhesion played a more important role.

When the effect of thermal annealing over the storage modulus was analyzed, it was found that at 40 ºC (i.e., below T_g), this property slightly decreased in all CM composites. Similar behavior was reported in Pérez-Fonseca *et al.* (2016) for injection molded PLA and its agave biocomposites. However, an opposite trend occurred for RM samples: the storage modulus increased by up to 45 % after thermal annealing. Additionally, it was observed that the significant storage modulus drop above T_g was almost eliminated by the thermal treatment for all the materials. The same behavior was reported by Mathew *et al.* (2006), Auras *et al.* (2010), Way *et al.* (2013), and Pérez-Fonseca *et al.* (2016). Therefore, this increase of storage modulus between 60 ºC and 80 ºC for the PLA and its biocomposites may imply an improvement in their thermal stability, opening potential applications at relatively higher temperatures (larger service window).

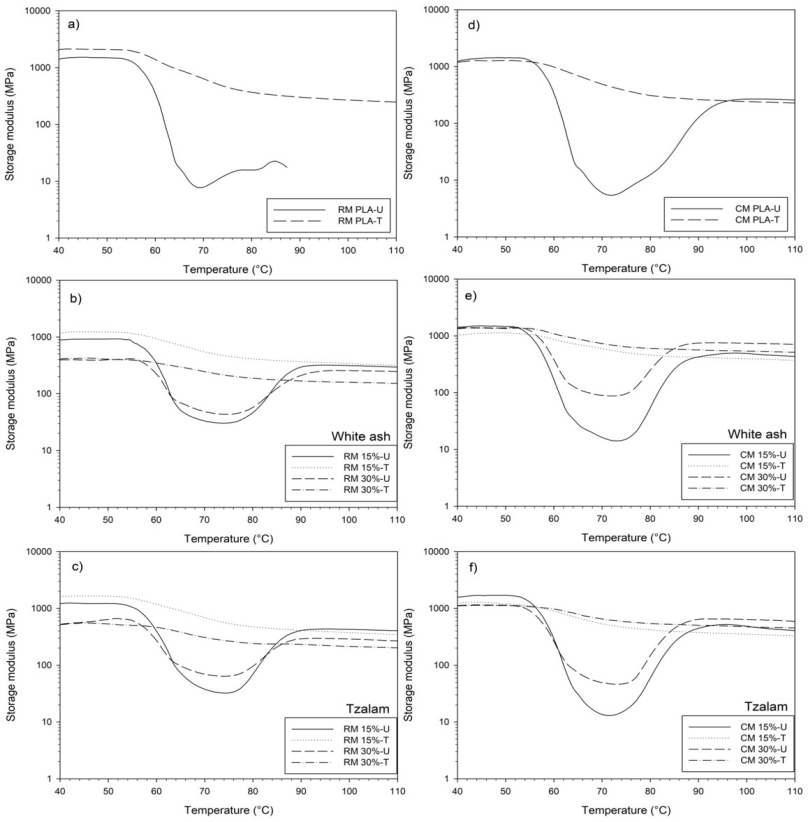

Figure 3: Storage modulus of rotomolded (a), (b), (c) and compression-molded (d), (e), (f) PLA and PLA/wood biocomposites (U: untreated; T: treated).

Charpy impact strength

Figure 4 shows the effect of thermal annealing on the impact strength of PLA and its biocomposites. The neat PLA had a value of 26 J/m for both RM and CM samples since the processing method did not produce significant density changes in the neat PLA. However, the incorporation of wood particles to rotomolded PLA reduced the impact strength to 20 J/m and 17 J/m for the white ash and tzalam biocomposites. For the compression-molded samples, the biocomposites' impact strength was similar to the neat PLA with 27 J/m and 24 J/m for 30 % wt. white ash and tzalam. This lower impact strength in RM samples has been previously reported by Cisneros-López *et al.* (2018) and González-López *et al.* (2019). It was related to a combination of poor interfacial stress transfer due to the wood/PLA incompatibility and higher porosity/lower density of rotomolded biocomposites than compression molded ones. The effect of thermal annealing was higher for the neat PLA, showing an impact strength increase of 142 % and 111 % (63 J/m and 55 J/m) for RM and CM neat PLA. This improvement can be related to increased crystallinity achieved by the thermal treatment (Perego *et al.* 1996, Pérez-Fonseca *et al.* 2016).

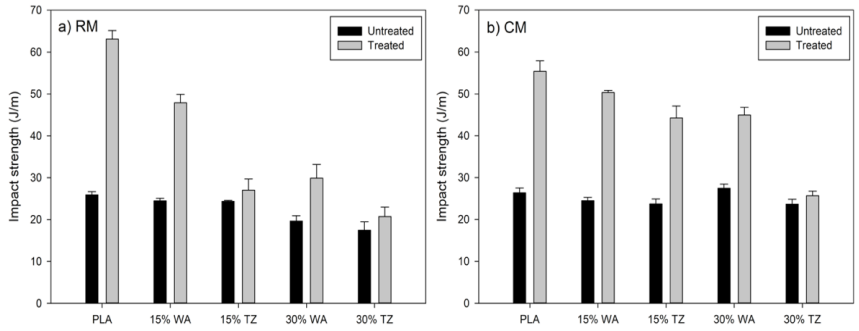

Figure 4: (a) Impact strength of rotomolded and (b) compression-molded PLA and PLA/wood biocomposites (WA: white ash; TZ: tzalam).

Thermal annealing increased the impact strength of the CM white ash biocomposites. In this case, the impact strength increased to 50 J/m and 44 J/m at 15 % and 30 % wt. of particle contents, respectively. Similarly, the CM tzalam biocomposites' impact strength increased to 44 J/m at 15 % wt., while no variation was observed at 30 % wt. The different behavior between both types of wood can be related to their chemical composition and interaction with the matrix (PLA). Tzalam has a higher extractables content (24 %) than white ash (15 %) (Pickering 2008, Rodríguez-Jiménez *et al.* 2019), which non-polar components help the interaction/adhesion with the PLA matrix (Mohanty *et al.* 2005). In the case of impact strength, the poor interfacial adhesion between the biopolymer and the wood particles makes the fracture path longer, increasing the absorbed energy (Martín del Campo *et al.* 2020).

The effect of thermal annealing on the RM biocomposites was similar to those of CM samples. Nevertheless, the impact strength increase was lower because of the higher porosity in RM biocomposites. Although the neat PLA achieved the highest impact strength with thermal annealing, the biocomposites with thermal annealing still achieved better properties than the untreated neat PLA.

Tensile and flexural properties

Tensile and flexural results are presented in Table 3. Tensile modulus of CM samples showed that wood addition caused an increase of 15 % and 25 % for 30 % wt. white ash and tzalam biocomposites, associated with wood particles' high stiffness (Pérez-Fonseca *et al.* 2015). However, in RM samples, the wood particles caused a decrease in tensile modulus, once again due to low particle dispersion, agglomeration, and lower density. Similar behavior was observed in flexural modulus results for both CM and RM samples. Even when it is well known that natural fibers possess high flexural modulus, the low wood/matrix compatibility, and the particle agglomeration can decrease this property in composites materials (Pérez-Fonseca *et al.* 2015, Robledo-Ortíz *et al.* 2021). The thermal annealing treatment did not significantly affect the tensile and flexural modulus since the biocomposites' values are similar to those of the untreated materials.

It was expected that tensile and flexural strengths were reduced with the addition of both kinds of wood since no coupling agent was used, which produced materials with lower density than neat PLA (Martín del Campo *et al.* 2020). Tensile and flexural strengths of neat PLA were 40 MPa and 80 MPa and decreased to 25 MPa and 50 MPa for the biocomposites. Thermal annealing caused decreases in tensile and flexural strengths. As mentioned, when materials are subjected to thermal treatments, recrystallization occurs, producing an increase in stiffness. This effect has been previously reported in Pérez-Fonseca *et al.* (2016).

Table 3: Flexural and tensile properties, and water absorption of PLA and its biocomposites produced by compression and rotational molding before and after thermal annealing (WA: white ash; TZ: tzalam).

Process	Thermal annealing at 100 °C	Time (min)	Flexural strength (MPa)*	Flexural modulus (MPa)*	Tensile strength (MPa)*	Tensile modulus (MPa)*	Water absorption at 672 h (%)*
Compression molding	PLA	0	88	3935	42	1264	0,6
		40	55	4016	21	1320	0,4
	15 % WA	0	60	3730	26	1373	9,5
		40	31	3388	14	1382	8,9
	30 % WA	0	48	3669	21	1430	14,3
		40	28	3375	14	1449	16,8
	15 % TZ	0	53	4071	25	1470	5,4
		40	25	3446	15	1413	5,9
	30 % TZ	0	37	3216	22	1577	9,6
		40	29	3897	16	1521	9,1
Rotational molding	PLA	0	79	3417	44	1233	0,6
		40	55	3895	34	1357	0,4
	15 % WA	0	52	3016	29	1246	10,1
		40	42	3267	21	1232	9,6
	30 % WA	0	23	1347	15	804	28,2
		40	18	1415	10	862	26,8
	15 % TZ	0	51	3392	26	1269	7,4
		40	38	3595	22	1312	6,6
	30 % TZ	0	22	1563	19	1166	14,6
		40	14	1312	9	1096	15,9

*All are average values with less than 10 % of standard deviation.

However, it is important to mention that even when it was found a significant decrease in flexural and tensile strength, the values are still competitive with those of polyethylene (flexural strength = 23 MPa, tensile strength 21 MPa), which is the most used polymer for rotomolding processes (95 % of the worldwide roto-molded parts) (Robledo-Ortíz *et al.* 2021).

Water absorption and accelerated weathering

Water absorption results are also shown in Table 3. The equilibrium in the water absorption was reached at 672 h or less. The maximum water absorption of pure PLA was around 0,6 % before thermal treatment and 0,4 % after the treatment regardless of the processing method. The slight difference in the treated PLA can be associated with the polymer chains' rearrangement during the recrystallization. As expected, the materials' hydrophilicity increased by adding both kinds of wood due to the high amounts of hydroxyl groups, being more evident at 30 % wt. of wood particles.

However, tzalam biocomposites absorbed less water than white ash biocomposites. This behavior is related to the different chemical compositions, especially with the higher non-polar extractables content in tzalam, making it less hydrophilic (Metsä-Kortelainen *et al.* 2006). Due to the absence of shear stresses during rotomolding, the blending of the components is not optimal, causing the formation of gaps that ease the water diffusion into the biocomposite. This behavior was clear in biocomposites with 30 % wt. of wood particles, e.g., compression-molded 30 % WA biocomposites had a water absorption of 14 %, while the same material but prepared by rotomolding absorbed 28 % of water. Similar results were found with tzalam particles. The thermal annealing produced only small water absorption differences compared with untreated samples, once again related to the polymer chains' rearrangement.

The behavior of PLA and its biocomposites was also studied under accelerated weathering to determine any changes in these materials' long-term properties. This information would be useful to increase their range of applications and their lifetime (Gunjal *et al.* 2020, González-López *et al.* 2020). Regardless of the processing method, the materials that were not subjected to thermal annealing presented significant changes in their dimensional stability after accelerated weathering. Figure 5 shows typical examples of these modifications, especially buckling in the biocomposites. This buckling of untreated samples is due to the softening of the PLA matrix around 60 ºC as previously discussed via DMTA (Figure 3). The thermal annealing was very efficient at increasing the crystallinity (Table 2) and the stiffness (Figure 3), thus improving the dimensional stability as temperature increases. Similar behavior was reported by Sawpan *et al.* (2019), where they observed deformation in their PLA samples after 768 h of accelerated weathering.

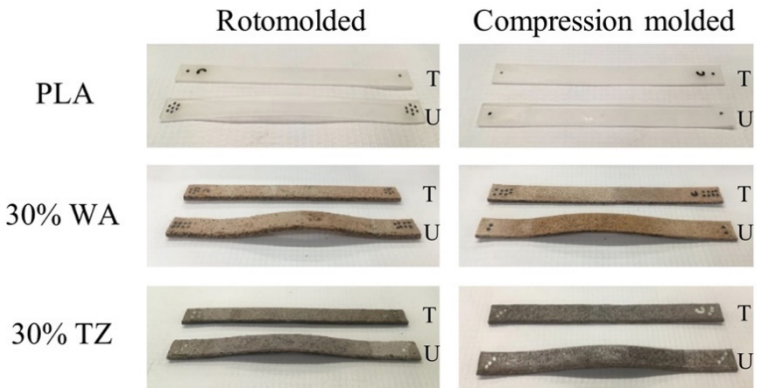

Figure 5: Dimensional stability of neat PLA and its biocomposites at 30 % wt. of white ash (WA) or tzalam (TZ) content (T: treated; U: untreated).

However, they reported that this buckling did not occur in the biocomposites because of hemp fibers addition. This difference in the dimensional stability of the PLA biocomposites can also be related to the characteristics of the lignocellulosic reinforcements, such as fiber dimensions and their aspect ratio (L/D), which is much higher for hemp fibers (>10) than for our white ash (3,1) and tzalam (2,7) particles.

Table 4 reports the crystallinity (X_c) of the materials after being exposed to accelerated weathering, where important changes were observed. It was found that the crystallinity of untreated PLA increased up to 38 % for either RM or CM; meanwhile, all the untreated biocomposites reach X_c, similar to those observed for the treated biocomposites (around 50 %). It has been reported that the conditions inside the weathering machines (humidity and temperatures around 50 ºC to 60 ºC) can lead to a reorganization of the PLA chains inducing cold crystallization (Sawpan *et al.* 2019). Also, Yatigala *et al.* (2018) reported that UV degradation mainly affects the amorphous regions of PLA so that crosslinking can occur in the imperfect crystalline regions and, consequently, increase its crystallinity.

Table 4: Crystallinity of PLA and its biocomposites before and after accelerated weathering

Rotomolded			Compression-molded		
Sample	Before	After	Sample	Before	After
	X_c (%)	X_c (%)		X_c (%)	X_c (%)
PLA-U	14	38	PLA-U	19	38
PLA-T	54	50	PLA-T	56	53
15 % WA-U	16	57	15 % WA-U	20	61
15 % WA-T	47	53	15 % WA-T	60	56
15 % TZ-U	18	60	15 % TZ-U	27	58
15 % TZ-T	49	55	15 % TZ-T	53	53
30 % WA-U	20	54	30 % WA-U	28	58
30 % WA-T	52	55	30 % WA-T	56	56
30 % TZ-U	20	53	30 % TZ-U	23	52
30 % TZ-T	54	56	30 % TZ-T	60	49

WA: white ash; TZ: tzalam; U: untreated; T: treated.

Figure 6 presents the DMTA results of PLA before and after accelerated weathering. The significant drop of around 60 ºC for the untreated PLA was more limited after weathering. This change was attributed to the increased crystallinity due to thermal annealing during weathering, which made PLA more stable and able to sustain higher temperatures. On the other hand, slight storage modulus decreases were observed for treated RM and CM PLA after weathering, which can be related to photo and hydrolytic degradation of PLA (Kaynak and Sari 2016). Moreover, no significant changes were observed below T_g, indicating that the weathering influence was mainly on the crystallization of the PLA amorphous region.

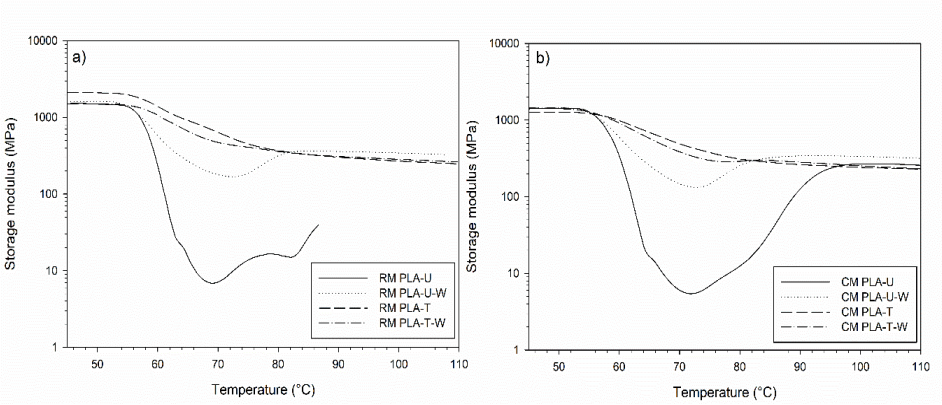

Figure 6: Storage modulus of rotomolded (a) and compression-molded (b) PLA before and after accelerated weathering (U: untreated; T: treated; W: weathered).

Similar DMA results to those of the neat PLA were observed for the RM (Figure 7) and CM (Figure 8) biocomposites after accelerated weathering. The untreated samples did not show significant softening around 60 ºC, once again due to a thermal annealing process occurring during weathering. However, considerable storage modulus losses due to weathering were observed below T_g for the untreated RM biocomposites, as well as for the complete curve for treated ones. For 30 % wt. of wood content at 50 ºC, the storage modulus of untreated RM biocomposites decreased from 395 MPa to 238 MPa for white ash and from 648 MPa to 262 MPa for tzalam, while for the treated RM biocomposites, the values were from 406 MPa to 246 MPa for white ash and 529 MPa to 258 MPa for tzalam. As expected, the biocomposites produced by compression molding have better resistance to the accelerated weathering conditions showing lower storage modulus decreases and more similarity to the neat PLA. This behavior can be related to the higher porosity, lower wood particle dispersion, and lower density of RM biocomposites that made water penetration more accessible, i.e., higher water absorption (as observed in Table 3) and possible swelling effect during weathering, promoting the hydrolysis of PLA chains (Islam *et al.* 2010). Niemczyk *et al.* (2019) also reported that particle agglomeration could accelerate polymer degradation due to many structural defects facilitating the oxygen permeability between the polymer chains. Nevertheless, it is important to notice that, in general, the treated biocomposites showed higher storage modulus after accelerated weathering, confirming their better dimensional and thermo-mechanical stability.

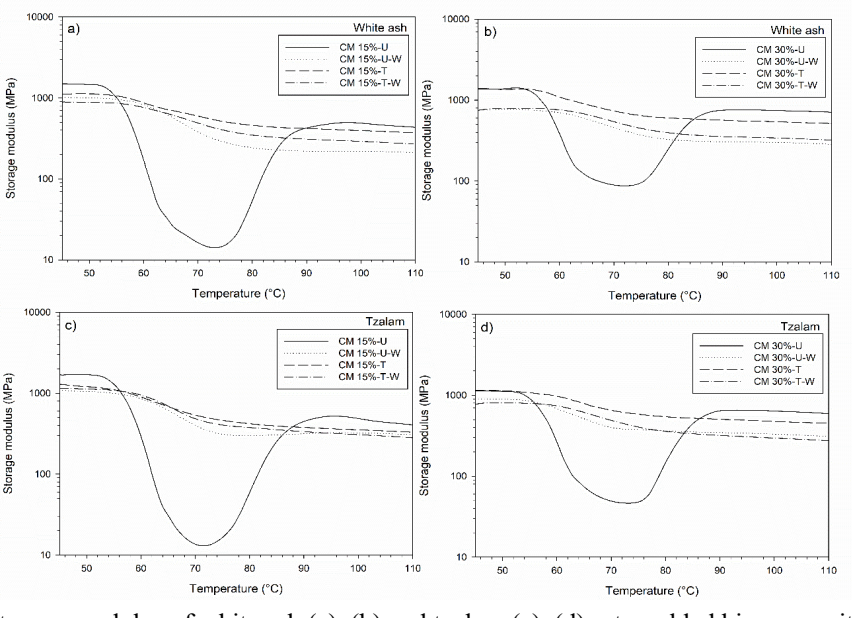

Figure 7: Storage modulus of white ash (a), (b) and tzalam (c), (d) rotomolded biocomposites before and after accelerated weathering (U: untreated; T: treated; W: weathered).

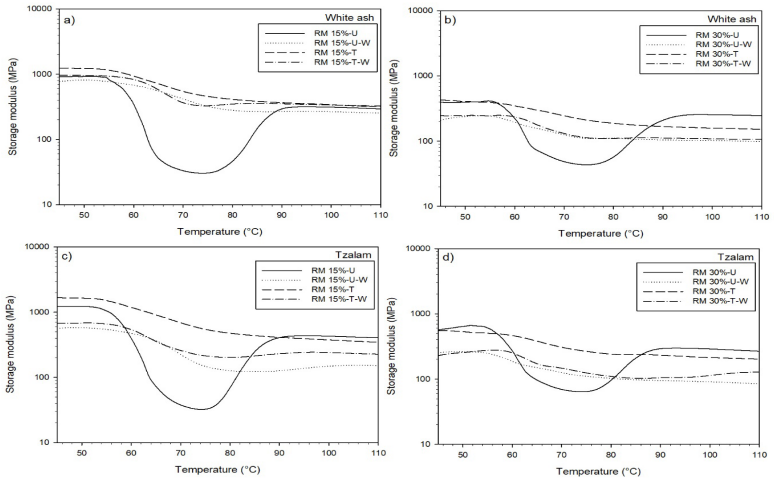

Figure 8: Storage modulus of white ash (a), (b) and tzalam (c), (d) compression-molded biocomposites before and after accelerated weathering (U: untreated; T: treated; W: weathered).

The results of impact strength before and after accelerated weathering are shown in Figure 9. Despite the processing method, it can be seen that the impact strength of untreated PLA and the untreated biocomposites did not significantly change after accelerated weathering. The latter could be related to a balance between the increased crystallinity produced by thermal annealing during weathering and polymer/fiber degradation. On the other hand, these crystallinity increases were not observed in treated PLA and treated biocomposites (Table 4), which showed important impact strength loss after weathering. This behavior suggests that polymer/fiber degradation is the main process during the accelerated weathering of treated samples. Nevertheless, lower decreases were observed at higher wood contents, which was related to the fact that the thermal annealing effect was less important under these conditions. However, limited impact strength changes after weathering between materials with and without thermal treatment are observed, which can be acceptable in terms of dimensional and thermo-mechanical stability of treated materials.

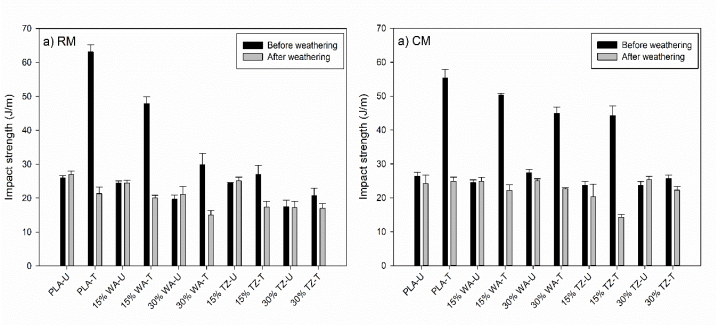

Figure 9: Impact strength of rotomolded (a) and compression-molded (b) PLA and PLA/wood biocomposites before and after accelerated weathering (WA: white ash; TZ: tzalam; U: untreated; T: treated).

CONCLUSIONS

The thermal annealing and wood addition (tzalam or white ash) are excellent options to enhance the crystallinity and impact strength, as well as the thermal and dimensional stability of PLA produced by rotational (RM) and compression (CM) molding. In general, higher crystallinity and mechanical properties were obtained for CM biocomposites than RM biocomposites, especially at high fiber content due to better compaction (higher density and lower defects and porosity).

The optimum thermal treatment was at 100 ºC for 40 min to maximize crystallinity for neat PLA. The thermal annealing enabled the PLA and PLA/wood biocomposites to have better thermo-mechanical stability at higher temperatures (especially above T_g). Since PLA is a brittle material, higher impact strength was necessary for a wider range of applications. This improvement in impact strength was successfully achieved by the thermal annealing treatment as the values improved by 142 % and 111 % for RM and CM neat PLA,

respectively. Samples subjected to accelerated weathering and thermal annealing had enhanced dimensional stability by restraining buckling during weathering under the conditions tested.

Overall, it can be concluded that wood particle addition and thermal annealing are easy strategies to produced biodegradable composite materials with competitive mechanical properties, reducing costs, which may increase their possible industrial and commercial applications.

ACKNOWLEDGMENTS

The authors acknowledge the State Council of Science and Technology of Jalisco (COECyTJAL) for the grant FODECIJAL 8107-2019. One of the authors (V.O. Ramírez-Herrera) acknowledges the financial support of the Mexican National Council for Science and Technology (CONACyT #851515) for her scholarship. Also, the technical help from Mr. Yann Giroux was highly appreciated.

REFERENCES

Adefisan, O.O.; McDonald, A.G. 2019. Evaluation of the strength, sorption and thermal properties of bamboo plastic composites. *Maderas-Cienc Tecnol* 21(1): 3-14. http://dx.doi.org/10.4067/S0718-221X2019005000101

Altuntas, E.; Aydemir, D. 2019. Effects of wood flour on the mechanical, thermal and morphological properties of poly(l-lactic acid)-chitosan biopolymer composites. *Maderas-Cienc Tecnol* 21(4): 611-618. http://dx.doi.org/10.4067/S0718-221X2019005000416

ASTM. 2013. Standard practice for fluorescent ultraviolet (UV) lamp apparatus exposure of plastics. ASTM D4329-13. 2013. ASTM: West Conshohocken, PA, USA.

ASTM. 2014. Standard test method for tensile properties of plastics. ASTM D638-14. 2014. ASTM: West Conshohocken, PA, USA.

ASTM. 2017. Standard test methods for flexural properties of unreinforced and reinforced plastics and electrical insulating materials. ASTM D790-17. 2017. ASTM: West Conshohocken, PA, USA.

ASTM. 2018. Standard test method for determining the Charpy impact resistance of notched specimens of plastics. ASTM D6110-18. 2018. ASTM: West Conshohocken, PA, USA.

ASTM. 2018. Standard test method for water absorption of plastics. ASTM D570-18. 2018. ASTM: West Conshohocken, PA, USA.

Arias, A.; Heuzey, M.C.; Huneault, M.A. 2013. Thermomechanical and crystallization behavior of polylactide-based flax fiber biocomposites. *Cellulose* 20: 439-452. https://dx.doi.org/10.1007/s10570-012-9836-8

Auras, R.; Lim, L.T.; Selke, S.E.M.; Tsuji, H. 2010. *Poly (lactic acid): synthesis, structures, properties, processing and applications*. John Wiley & Sons, Inc: USA. ISBN 9780470649848. 528p. https://dx.doi.org/10.1002/9780470649848

Cisneros-López, E.O.; Pérez-Fonseca, A.A.; González, Y.; González-Núñez, R.; Rodrigue, D.; Robledo-Ortíz, J.R. 2018. Polylactic acid-agave fiber biocomposites produced by rotational molding: A comparative study with compression molding. *Adv Polym Tech* 37(7): 2528-2540. https://dx.doi.org/10.1002/adv.21928

Dong, Y.; Ghataura, A.; Takagi, H.; Haroosh, H.; Nakagaito, A.; Lau, K.T. 2014. Polylactic acid (PLA) biocomposites reinforced with coir fibres: Evaluation of mechanical performance and multifunctional properties. *Compos Part A-Appl S* 63: 76-84. https://dx.doi.org/10.1016/j.compositesa.2014.04.003

Faludi, G.; Dora, G.; Renner, K.; Móczó, J.; Pukánszky, B. 2013. Improving interfacial adhesion in PLA/wood biocomposites. *Compos Sci Technol* 89: 77-82. https://dx.doi.org/10.1016/j.compscitech.2013.09.009

Ferrer-Balas, D.; Maspoch, M.L.; Martinez, A.B.; Santana, O.O. 2001. Influence of annealing on the microstructural, tensile and fracture properties of polypropylene films. *Polymer* 42(4): 1697-1705. https://dx.doi.org/10.1016/S0032-3861(00)00487-0

Frone, A.N.; Berlioz, S.; Chailan, J.F.; Panaitescu, D.M. 2013. Morphology and thermal properties of PLA-cellulose nanofibers composites. *Carbohyd Polym* 91(1): 377-384. https://dx.doi.org/10.1016/j.carbpol.2012.08.054

González-López, M.E.; Robledo-Ortíz, J.R.; Manríquez-González, R.; Silva-Guzman, J.A.; Pérez-Fonseca, A.A. 2018. Polylactic acid functionalization with maleic anhydride and its use as coupling agent in natural fiber biocomposites: a review. *Compos Interface* 25(5-7): 515-538. https://dx.doi.org/10.1080/09276440.2018.1439622

González-López, M.E.; Pérez-Fonseca, A.A.; Cisneros-López, E.O.; Manríquez-González, R.; Ramírez-Arreola, D.E.; Rodrigue, D.; Robledo-Ortíz, J.R. 2019. Effect of maleated PLA on the properties of rotomolded PLA-agave fiber biocomposites. *J Polym Environ* 27: 61-73. https://dx.doi.org/10.1007/s10924-018-1308-2

González-López, M.E.; Martín del Campo, A.S.; Robledo-Ortíz, J.R.; Arellano, M.; Pérez-Fonseca, A.A. 2020. Accelerated weathering of poly (lactic acid) and its biocomposites: A review. *Polym Degrad Stabil* 179: 109290. https://dx.doi.org/10.1016/j.polymdegradstab.2020.109290

Greco, A.; Maffezzoli, A.; Forleo, S. 2014. Sintering of PLLA powders for rotational molding. *Thermochim Acta* 582: 59-67. https://dx.doi.org/10.1016/j.tca.2014.03.005

Greco, A.; Maffezzoli, A. 2015. Analysis of the suitability of poly(lactic acid) in rotational molding process. *Adv Polym Tech* 34 (3): 1-8. https://dx.doi.org/10.1002/adv.21505

Greco, A.; Maffezzoli, A. 2017. Rotational molding of poly(lactic acid): Effect of polymer grade and granulometry. *Adv Polym Tech* 36 (4): 477-482. https://dx.doi.org/10.1002/adv.21630

Gunjal, J.; Aggarwal, P.; Chauhan, S. 2020. Changes in colour and mechanical properties of wood polypropylene composites on natural weathering. *Maderas-Cienc Tecnol* 22(3): 325-334. http://dx.doi.org/10.4067/S0718-221X2020005000307

Islam, M.S.; Pickering, K.L.; Foreman, N.J. 2010. Influence of accelerated ageing on the physico-mechanical properties of alkali-treated industrial hemp fibre reinforced poly (lactic acid) (PLA) composites. *Polym Degrad Stabil* 95(1): 59-65. https://dx.doi.org/10.1016/j.polymdegradstab.2009.10.010

Kaynak, C.; Sari, B. 2016. Accelerated weathering performance of polylactide and its montmorillonite nanocomposite. *Appl Clay Sci* 121-122: 86-94. https://dx.doi.org/10.1016/j.clay.2015.12.025

Kim, H.S.; Lee, B.H.; Choi, S.W. 2007. The effect of types of maleic anhydride-grafted polypropylene (MAPP) on the interfacial adhesion properties of bio-flour-filled polypropylene composites. *Compos Part A-Appl S* 38(6): 1473-1482. https://dx.doi.org/10.1016/j.compositesa.2007.01.004

Mahfoudh, A.; Cloutier, A; Rodrigue, D. 2013. Characterization of UHMWPE/wood composites produced via dry-blending and compression molding. *Polym Composite* 34(4): 510-516. https://dx.doi.org/10.1002/pc.22455

Martín del Campo, A.S.; Robledo-Ortíz, J.R.; Arellano, M.; Rabelero, M.; Pérez-Fonseca, A.A. 2020. Accelerated weathering of polylactic acid/agave fiber biocomposites and the effect of fiber–matrix adhesion. *J Polym Environ* 29: 937-947. https://dx.doi.org/10.1007/s10924-020-01936-z

Mathew, A.P.; Oksman, K.; Sain, M. 2006. The effect of morphology and chemical characteristics of cellulose reinforcements on the crystallinity of polylactic acid. *J Appl Polym Sci* 101(1): 300-310. https://dx.doi.org/10.1002/app.23346

Metsä-Kortelainen, S.; Antikainen, T.; Viitaniemi, P. 2006. The water absorption of sapwood and heartwood of Scots pine and Norway spruce heat-treated at 170 °C, 190 °C, 210 °C and 230 °C. *Holz Roh Werkst* 64: 192-197. https://dx.doi.org/10.1007/s00107-005-0063-y

Mohanty, A.K.; Misra, M.; Drzal, L.T. 2005. *Natural Fibers, Biopolymers, and Biocomposites*. 896p. CRC Press: USA. ISBN 9780429211607. https://dx.doi.org/10.1201/9780203508206

Niemczyk, A.; Dziubek, K.; Grzymek, M.; Czaja, K. 2019. Accelerated laboratory weathering of polypropylene composites filled with synthetic silicon-based compounds. *Polym Degrad Stabil* 161: 30-38. https://dx.doi.org/10.1016/j.polymdegradstab.2019.01.005

Perego, G.; Cella, G.D.; Bastlol, C. 1996. Effect of molecular weight and crystallinity on poly (lactic acid) mechanical properties. *J Appl Polym Sci* 59(1): 37-43. https://dx.doi.org/10.1002/(SICI)1097-4628(19960103)59:1<37::AID-APP6>3.0.CO;2-N

Pérez-Fonseca, A.A.; Robledo-Ortíz, J.R.; González-Núñez, R.; Rodríguez, D. 2016. Effect of thermal annealing on the mechanical and thermal properties of polylactic acid-cellulosic fiber biocomposites. *J Appl Polym Sci* 133(31): 1-9. https://dx.doi.org/10.1002/app.43750

Pérez-Fonseca, A.A.; Robledo-Ortíz, J.R.; Moscoso-Sánchez, F.J.; Fuentes-Talavera, F.J.; Rodrigue, D.; González-Núñez, R. 2015. Self-hybridization and coupling agent effect on the properties of natural fiber/HDPE composites. *J Polym Environ* 23: 126-136. https://dx.doi.org/10.1007/s10924-014-0706-3

Petchwattana, N.; Covavisaruch, S.; Petthai, S. 2014. Influence of talc particle size and content on crystallization behavior, mechanical properties and morphology of poly (lactic acid). *Polym Bull* 71: 1947-1959. https://dx.doi.org/10.1007/s00289-014-1165-7

Piekarska, K.; Piorkowska, E.; Krasnikova, N.; Kulpinski, P. 2017. Polylactide composites with waste cotton fibers: Thermal and mechanical properties. *Polym Composite* 35(4): 747-751. https://dx.doi.org/10.1002/pc.22717

Pickering, K.L. 2008. *Properties and performance of natural-fibre composites*. 576p. Woodhead Publishing: England. ISBN 9781845692674. https://dx.doi.org/10.1533/9781845694593

Robledo-Ortíz, J.R.; González-López, M.E.; Martín del Campo, A.S.; Peponi, L.; González-Nuñez, R.; Rodrigue, D.; Pérez-Fonseca, A.A. 2021. Fiber-matrix interface improvement via glycidyl methacrylate compatibilization for rotomolded poly (lactic acid)/agave fiber biocomposites. *J Compos Mater* 55(2): 201-212. https://dx.doi.org/10.1177/0021998320946821

Robledo-Ortíz, J.R.; González-López, M.E.; Rodrigue, D.; Gutiérrez-Ruiz, J.F.; Prezas-Lara, F.; Pérez-Fonseca, A.A. 2020. Improving the compatibility and mechanical properties of natural fibers/green polyethylene biocomposites produced by rotational molding. *J Polym Environ* 28: 1040-1049. https://dx.doi.org/10.1007/s10924-020-01667-1

Rodríguez-Jiménez, S.; Duarte-Aranda, S.; Canché-Escamilla, G. 2019. Chemical composition and thermal properties of tropical wood from the Yucatán dry forests. *Bioresources* 14(2): 2651-2666. https://dx.doi.org/10.15376/biores.14.2

Sawpan, M.A.; Islam, M.R.; Hossain-Beg M.R.; Pickering, K. 2019. Effect of accelerated weathering on physico-mechanical properties of polylactide bio-composites. *J Polym Environ* 27: 942-955. https://dx.doi.org/10.1007/s10924-019-01405-2

Srithep, Y.; Nealey, P.; Turng, L.S. 2013. Effects of annealing time and temperature on the crystallinity and heat resistance behavior of injection-molded poly (lactic acid). *Polym Eng Sci* 53(3): 580-588. https://dx.doi.org/10.1002/pen.23304

Way, C.; Wu, D.Y.; Cram, D.; Dean, K.; Palombo, E. 2013. Processing stability and biodegradation of polylactic acid (PLA) composites reinforced with cotton linters or maple hardwood fibres. *J Polym Environ* 21(1): 54-70. https://dx.doi.org/10.1007/s10924-012-0462-1

Yang, T.C.; Hung, K.C.; Wu, T.L.; Wu, T.M.; Wu, J.H. 2015. A comparison of annealing process and nucleating agent (zinc phenylphosphonate) on the crystallization, viscoelasticity, and creep behavior of compression-molded poly(lactic acid) blends. *Polym Degrad Stabil* 121: 230-237. https://dx.doi.org/10.1016/j.polymdegradstab.2015.09.012

Yatigala, N.S.; Bajwa, D.S.; Bajwa, S.G. 2018. Compatibilization improves performance of biodegradable biopolymer composites without affecting UV weathering characteristics. *J Polym Environ* 26: 4188-4200. https://dx.doi.org/10.1007/s10924-018-1291-7